Supplementary Information for optomechanical ring resonator for efficient microwave-optical frequency conversion

I-Tung Chen,[1] Bingzhao Li,[1] Seokhyeong Lee,[1] Srivatsa Chakravarthi,[2] Kai-Mei Fu,[1,2] and Mo Li[1,2,*]

[1] *Department of Electrical and Computer Engineering, University of Washington, Seattle, WA 98115, USA*

[2] *Department of Physics, University of Washington, Seattle, WA 98115, USA*

SI.1. COUPLED-MODE THEORY (CMT) ANALYSIS

We employ the coupled-mode theory (CMT) to analyze the OMR system. The electric field propagating in the OMR experiences a perturbed dielectric medium ($\Delta\varepsilon$) hence induces a perturbed polarization field:

$$\Delta\mathbf{P} = \Delta\varepsilon(x,y,z)\mathbf{E}_i(x,y)e^{i(\omega t-\beta_i z)}.$$

where β_i is the propagating wavevector of the i-th mode, $E_i(x,y)$ is the normal mode electric field of the i-th mode. The mechanical perturbation of the permittivity $\Delta\varepsilon$ consists of contributions from the moving boundary effect[1] and the photoelastic effect[2] and can be described as

$$\Delta\varepsilon = \delta\varepsilon\cdot\mathbf{u} = -\underbrace{\mathbf{u}(x,y)\cdot\mathbf{n}(x,y)(\Delta\varepsilon'|\mathbf{E}_\parallel(x,y)|^2-\Delta\varepsilon'^{-1}|\mathbf{D}_\perp|^2)}_{\text{Moving boundary effect}}+\underbrace{\frac{\varepsilon\cdot p\mathbf{S}\cdot\varepsilon}{\varepsilon_0}}_{\text{Photoelastic effect}}$$

where $\mathbf{n}$ is the normal vector pointing from the dielectric 1 to dielectric 2; $\Delta\varepsilon' = \varepsilon_2-\varepsilon_1$ and $\Delta\varepsilon'^{-1} = \varepsilon_2^{-1}-\varepsilon_1^{-1}$; $\mathbf{E}_\parallel$ and $\mathbf{D}_\perp$ are the tangential electric field and perpendicular displacement field at the dielectric boundary; p is the photoelastic tensor and $\mathbf{S}$ is the strain tensor. The mechanical displacement field of the acoustic wave is:

$$\mathbf{u}(x,y,z,t) = \mathbf{u}(x,y)e^{i(\Omega t-Kz)}+\text{c.c.}$$

where Ω is the acoustic frequency, K is the acoustic wavevector. The optical field is expressed as:

$$\mathbf{E}_i(x,y,z,t) = A_i\mathbf{e}_i(x,y)e^{i(\omega t-\beta_i z)}+\text{c.c.}$$

where A_i is the electric field amplitude which is normalized to equal to the optical power P_i. Here, we only consider two relevant modes: $i=0$ for the TE_0 mode and $i=2$ for the TE_2. Defining the phase mismatch $\Delta\beta = \beta_0-\beta_2-K\neq 0$, the mode coupling equations are:

$$\frac{d}{dz}A_2(z) = -iG_{20}A_0(z)e^{-i\Delta\beta z} \tag{SI.1}$$

where the total coupling coefficient G_{20} is given by:

$$G_{20} = -\frac{\omega_2}{2}\frac{\int dA\mathbf{E}_2^*\cdot\delta\varepsilon\cdot\mathbf{u}(x,y)\cdot\mathbf{E}_0}{P_2}.$$

And,

$$\frac{d}{dz}A_0(z) = -iG_{02}A_2(z)e^{i\Delta\beta z} \tag{SI.2}$$

where

$$G_{02} = -\frac{\omega_0}{2}\frac{\int dA\mathbf{E}_0^*\cdot\delta\varepsilon\cdot\mathbf{u}^*(x,y)\cdot\mathbf{E}_2}{P_0}.$$

* Corresponding author: moli96@uw.edu

Since the coupling rate is proportional to the square root of the phonon flux $\sqrt{\Phi} = \sqrt{P_a/\hbar\Omega}$, we define the normalized coupling rate $g \equiv G/\sqrt{\Phi} = G_{20}/\sqrt{\Phi} = G_{02}/\sqrt{\Phi}$. The solutions of $A_0(z)$ and $A_2(z)$ in the general case when $\Delta\beta \neq 0$ are:

$$A_0(z) = A_0(0)[cos(sz) - \frac{i\Delta\beta}{2}\frac{sin(sz)}{s}]e^{i\Delta\beta z/2} \tag{SI.3}$$

$$A_2(z) = A_0(0)[-iG\frac{sin(sz)}{s}]e^{i\Delta\beta z/2}. \tag{SI.4}$$

where A_0 and A_2 are the normalized amplitudes of the two modes that are traveling in the OMR, and $s = \sqrt{G^2 + (\Delta\beta/2)^2}$. The coupled mode equations show that the acoustic coupling G facilitates the coupling between the TE_0 and TE_2 modes with oscillatory energy exchange and a coupling length of $1/s$.

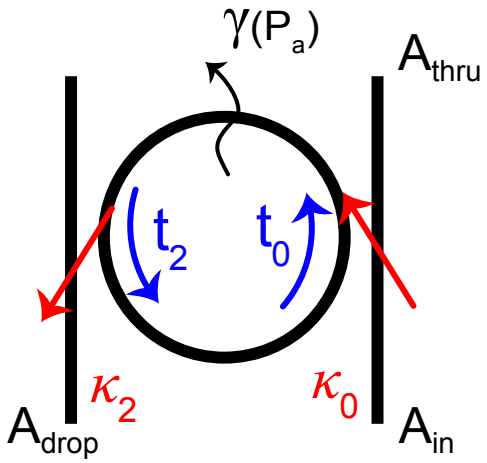

FIG. S1. **CMT model of the OMR.**

We now consider the intra-cavity optical field of the OMR. For the TE_0 mode, the optomechanical coupling to the TE_2 mode can be considered an additional loss, which depends on the acoustic wave power and changes the waveguide-ring coupling condition. Therefore, the intra-cavity loss is modulated by the acoustic power and can be expressed as $\gamma(P_a) = \gamma_0 + \Gamma sin(\pi\sqrt{P_a}/\sqrt{P_\pi})$, where γ_0 is the static intrinsic loss that is independent of the acoustic power and Γ is the strength of the optomechanically modulated loss. The output field amplitude at the drop port can be described with the standard ring resonator model using the transmission coefficient t_0, t_2 and the cross-coupling coefficient κ_0, κ_2, as shown in the Fig. S1

$$A_{drop}(P_a) = A_{in}\frac{\kappa_0\kappa_2\gamma(P_a)e^{-i\phi/2}}{1 - t_0t_2\gamma(P_a)e^{-i\phi}}$$

where ϕ is the round trip phase. At the resonance condition ($\phi = 2\pi$), the optomechanically modulated $\gamma(P_a)$ changes the output intensity as:

$$A^2_{drop}(P_a) = (A_{in}\frac{\kappa_0\kappa_2\gamma(P_a)}{1 - t_0t_2\gamma(P_a)})^2. \tag{SI.5}$$

We can perform a similar analysis on the circulating acoustic wave in the OMR. The intra-cavity acoustic field can be written as

$$u_{cav} = \frac{u_{in}\kappa_a}{1 - \gamma_a(P_a)t_ae^{-i\phi}}$$

where u_{in} is the input acoustic amplitude, u_{cav} is the intra-cavity acoustic amplitude, and κ_a is the coupling coefficient of the acoustic field from the bus waveguide to the OMR. Acoustic intrinsic loss coefficient is also modulated by the acoustic power and can be expressed as: $\gamma_a(P_a) = \gamma_{a0} + \Gamma_a sin(\pi\sqrt{P_a}/\sqrt{P_\pi})$, where γ_{a0} is the static acoustic loss

coefficient that is independent of the pump power, and Γ_a is the strength of the optomechanically modulated loss. Revisiting equations SI.3 and SI.4, we can replace the acoustic amplitude with intra-cavity acoustic amplitude and optical amplitude that is pumping on resonance ($\phi = 2\pi \cdot N$, $N = 1, 2, 3...$). The drop port optical field amplitude can be expressed as

$$A_{0-drop}(P_a,\ z) = A_{0-\mathrm{in}} \frac{\kappa_0 \kappa_2 \gamma(P_a)}{1 - t_0 t_2 \gamma(P_a)} \cdot [cos(s'z) - \frac{i\Delta\beta}{2} \frac{sin(s'z)}{s'}] e^{i\Delta\beta/2z} \tag{SI.6}$$

$$A_{2-drop}(P_a,\ z) = A_{0-\mathrm{in}} \frac{\kappa_0 \kappa_2 \gamma(P_a)}{1 - t_0 t_2 \gamma(P_a)} \cdot [-iG_{cav} \frac{sin(s'z)}{s'}] e^{-i\Delta\beta/2z} \tag{SI.7}$$

where $s' = \sqrt{(G_{cav})^2 + (\Delta\beta/2)^2}$, $G_{cav} = G \cdot \kappa_a/(1 - \gamma_a t_a)$, and A_{0-in} is the input optical amplitude from the waveguide.

SI.2. OPTOMECHANICAL CONVERSION EFFICIENCY CALCULATION

The optomechanical internal conversion efficiency is defined as

$$\eta_i = \frac{P_{TE_2}}{P_{TE_0}}$$

where P_{TE_2} is the optomechanical converted TE_2 mode power inside OMR, and P_{TE_0} is the power of TE_0 mode that coupled into OMR. P_{TE_0} is known because the laser power, the coupling efficiency of the grating coupler, and the transmission of the TE_0 through port are known. So, to calculate the optomechanical conversion efficiency, we need to obtain the P_{TE_2}. There are two methods to obtain P_{TE_2}, and thus η_i. The first method is by bookkeeping the optical power all the way from the RSA measured electrical power to the optical power inside the OMR. The second method is to use the fitting of equation SI.6 & SI.7 to obtain the intra-cavity field at $A_2(gD\pi\sqrt{P_{\pi/2}} = \pi/2)$ and calculated P_{TE_2} to obtain η_i. We will describe both methods in this section.

The Bookkeeping method

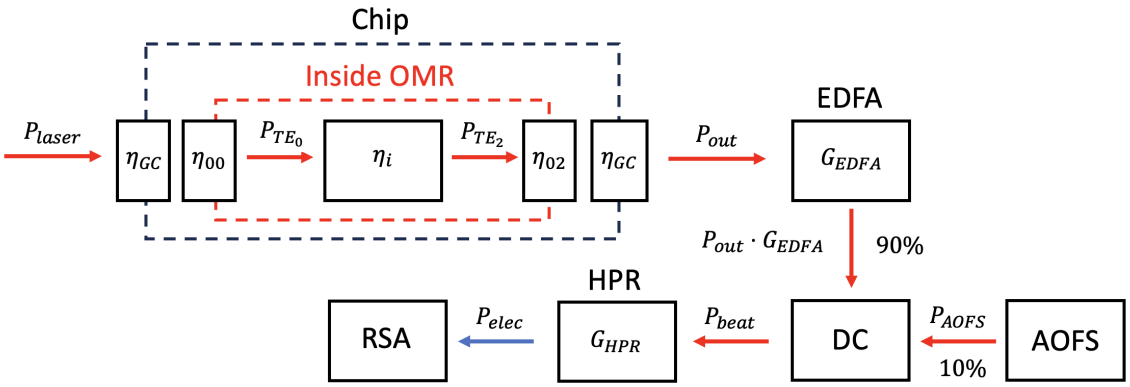

FIG. S2. TE_0**-to-**TE_2 **optomechanical conversion efficiency calculation flowchart.** The red arrows represent the optical signal, and the blue arrows represent the electrical signal. The input laser power P_{laser}, is coupled to the OMR through a grating coupler with coupling efficiency η_{GC} and the waveguide-to-OMR coupling efficiency η_{00}. The input TE_0 mode is then converted to TE_2 mode at the OMR with intrinsic efficiency η_i. The TE_2 mode is then coupled out of the OMR with efficiency η_{02} and out of the chip from the grating coupling with efficiency η_{GC}. The output TE_2 optical power is labeled as P_{out}. P_{out} is then amplified by EDFA with gain G_{EDFA} and beats with the AOFS in a directional coupler (DC). The beating optical signal P_{beat} is finally detected by the high-speed photoreceiver (HPR) and converted to electric signal P_{elec} and read out by the RSA.

The TE_2 optical power output from the OMR is first amplified by an erbium-doped fiber amplifier (EDFA), and combined with the acousto-optic frequency shifter (AOFS) reference signal, then converted to electrical power by the high-speed photoreceiver (HPR), and finally measured by the RSA, as shown in Fig. S2. We start the bookkeeping calculation from the RSA measured power. The conversion of the optical P_{optical} to electrical power P_{elec} via HPR can be expressed as

$$P_{\text{elec}} = (G_{\text{HPD}} \cdot P_{\text{beat}})^2 / R_{char}$$

where the voltage conversion gain of the HPR $G_{\text{HPR}} = 500$ V/W and the characteristic impedance $R_{char} = 50$ Ohm. And the optical power P_{beat} is the beating signal of P_{out} and P_{AOFS}, which can be expressed as

$$P_{\text{beat}} = \sqrt{0.9P_{\text{out}} \cdot G_{\text{EDFA}} \cdot 0.1P_{\text{AOFS}}}$$

where the gain from EDFA $G_{\text{EDFA}} = 9.6$ dB, the $P_{\text{AOFS}} = 0.038$ mW. G_{EDFA} had been calibrated using a power meter at 1550 nm therefore the gain is known. The pre-factors 0.9 and 0.1 are the table-top directional coupler's transmission coefficient that is used to combine the AOFS and the device output signal.

$$P_{\text{out}} = \frac{P_{\text{elec}} R_{char} / G_{\text{HPR}}^2}{G_{\text{EDFA}} \cdot 0.9 \cdot 0.1 \cdot P_{AOFS}} \text{ (W)}$$

where $P_{\text{elec}} = -55$ dBm, the resulted $P_{\text{out}} = 6.16$ nW. Now, we can back-calculate the power inside the OMR by considering grating coupler efficiency η_{GC} and the TE_2 out-couple efficiency η_{02} using

$$P_{TE2} = \frac{P_{\text{out}}}{\eta_{GC}\eta_{02}}$$

where $\eta_{GC} = 3\%$ and $\eta_{02} = 3\%$, respectively. The resulted optomechanically converted TE_2 power in the OMR $P_{TE2} = 6.84$ μW. On the input side, the TE_0 power in the ring can be calculated as

$$P_{TE0} = P_{\text{laser}} \cdot \eta_{GC} \cdot \eta_{00}$$

where $P_{\text{laser}} = 12$ mW, $\eta_{GC} = 3\%$, and $\eta_{00} = 90\%$. The resulted input $P_{TE0} = 324$ μW, and the intrinsic optomechanical conversion efficiency $\eta_i = 2.1 \pm 0.1\%$ A optomechanical overall conversion efficiency of the device is defined as

$$\eta_{\text{tot}} = \frac{P_{\text{out}}}{P_{\text{laser}}}$$

where P_{out} is the output power at TE_2 port after the grating coupler, and P_{laser} is the laser input power, as shown in Fig. S2. The resulting $\eta_{tot} = 0.57 \times 10^{-6}$.

The CMT model fitting method

The optomechanical conversion efficiency can be extracted directly by taking the square ratio of equation (SI.6) and (SI.7). We fit $P_{02}(\Omega - \delta)$ from Fig. 4(e) in main text using equation (SI.7) with the parameter listed in tableS1. The fitted parameter is then used in equation (SI.6) to calculate the corresponding $A^2_{0-drop}(P_a)$. The measured data $P_{02}(\delta)$ in Fig. 4(d) is only a reference signal that is proportional to $A^2_{0-drop}(P_a)$, therefore, we rescale equation (SI.6) and plot the rescaled fitting in Fig. 4(d). To calculate the optomechanical internal conversion efficiency η_i, we plug in the fit parameters to equation (SI.6) at the critical acoustic power $P_a = 1.6$ mW, which yields a value of $A^2_{0-drop} = 2.94$ nW. A^2_{2-drop} can also be extracted in the same fashion using equation (SI.7). At $sin(s'z) = 1$, A^2_{2-drop} has a maximum value of 0.42 nW. The resulting $\eta_i = (A_{2-drop}/A_{0-drop})^2 = 6.9 \pm 1\%$, which is higher than the bookkeeping method. The fixed parameters are the known values in our system, including the coupling coefficient from bus waveguide to ring, and the optomechanically modulated loss. Both the experimental and the theoretical approaches produce similar conversion efficiencies that are consistent with each other.

Fixed parameters								Fit parameters	
A_{0-in} $(\sqrt{W})$	κ_0	κ_2	κ_a	γ_0	Γ	γ_{a0}	Γ_a	g $(mm^{-1}\sqrt{W^{-1}})$	$\Delta\beta$ (μm^{-1})
0.02	0.95	0.17	0.8	0.33	0.2	0.65	0.35	230	0.079

TABLE S1. Fitting parameters that are used to calculate g

We can also extract the optomechanical coupling coefficient g and the phase mismatch $\Delta\beta$ from the CMT fitting. Using the calculated optomechanical coefficient, we can calculate the conversion power for a unity conversion efficiency when $\Delta\beta = 0$ using

$$\sqrt{P_{\pi/2}}\,|_{\Delta\beta=0} = \frac{\sqrt{\hbar\Omega}}{2gD} = 0.01\sqrt{W}$$

the resulted power to achieve unity conversion efficiency when $\Delta\beta = 0$ is 0.1 mW.

Finite Element Method Simulations

Here we discuss the simulation of the presented optomechanical system and calculate the optomechanical coupling coefficient g_0. As stated above, the optomechanical coupling is facilitated through traveling waves in the presented OMR system, which is different from the previous standing-wave systems. Therefore, instead of simulating the whole OMR system, we simulate the acoustic and optical mode profile of a cross-section of the waveguide, as shown in the

main text Fig. 1. We use COMSOL 5.6 to simulate the cross-sectional mode profile and calculate g_0 from the moving boundary (MB) and the photoelastic (PE) contribution using the following expressions

$$\frac{g_0}{\sqrt{\hbar\Omega}} = \frac{G_{MB}}{\sqrt{P_a}} + \frac{G_{PE}}{\sqrt{P_a}} \text{ unit:} \frac{1}{\text{mm}\sqrt{\text{W}}}$$

where G_{MB} and G_{PM} are the optomechanical coupling coefficient contributed by the MB and PE effect, respectively. The following table provides the corresponding simulated value and the calculated g_0. The calculated

$$g_0/\sqrt{\hbar\Omega} = 574.3\ mm^{-1}\sqrt{W^{-1}}$$

which is roughly 2.5 times larger than the measured g_0 from data. The simulated $g_0/\sqrt{\hbar\Omega}$ has a $P_{\pi/2} = 0.02$ mW using the same OMR geometry as in the main text. Since the moving boundary effect dominates the coupling, we attribute the discrepancy in the $g_0/\sqrt{\hbar\Omega}$ to the refractive index difference between the BGaP and GaP.

$\omega_0/2\pi$ (THz)	$\omega_m/2\pi$ (GHz)	$G_{MB}/\sqrt{P_a}$ $(mm^{-1}\sqrt{W^{-1}})$	$G_{PE}/\sqrt{P_a}$ $(mm^{-1}\sqrt{W^{-1}})$	P_a (W)
190.80	2.56	-7.9	582.2	3.8×10^{-3}

TABLE S2. Parameters from FEM simulation

SI.3. PIEZO-OPTOMECHANICAL TRANSDUCTION EFFICIENCY

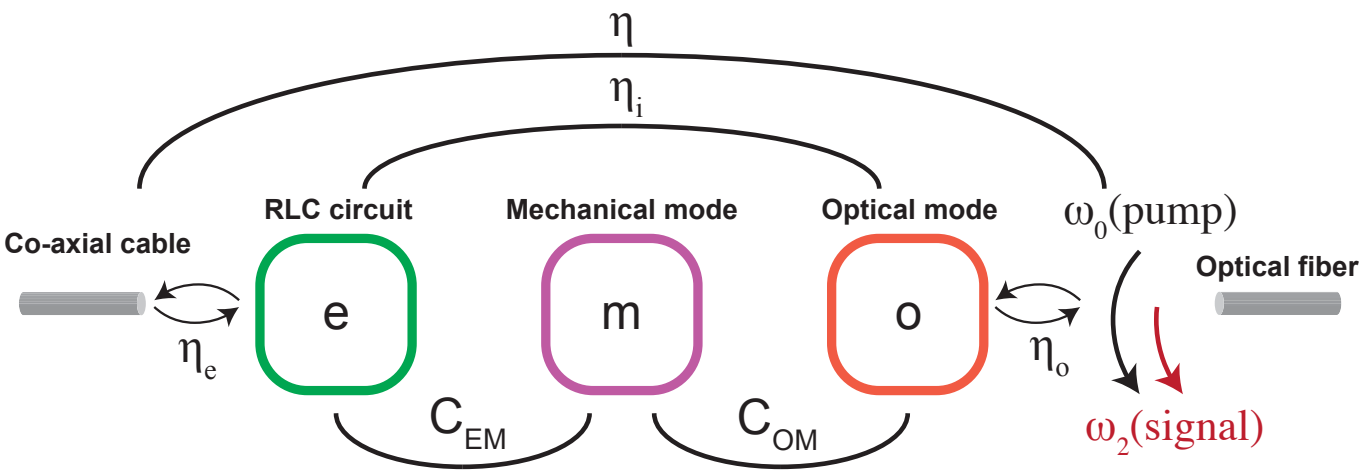

FIG. S3. **General schematic for microwave-to-optical conversion.**

A general schematic of the microwave-to-optical conversion of our device is shown in Fig. S3. Here, the microwave-to-optical conversion is a two stage conversion, where the microwave signal is coupled to the mechanical resonator via electromechanical coupling with coupling rate g_{EM}, and the mechanical resonator is coupled to the optical resonator via optomechanical coupling with coupling rate g_{OM}. In this section, we will characterize the key para maters related to the microwave-to-optical transduction. The following calculations are based on the work of Wu et al. [3], Han et al. [4] and Aspelmeyer et al. [5].

This section is structured as follows: in Section SI.3 A we examine the calculation of the cooperativities C_{EM} and C_{OM}, in Section SI.3 B we calculate the internal (η_i) and the total efficiency (η), and in Section SI.3 C we calculate the added noise of the optomechanical ring system

A. Cooperativities

A general form of the cooperativity is expressed as:

$$C_{ij} = \frac{4g_{ij}^2}{k_i k_j}$$

where i, j = (o, m, e) for one stage microwave-to-optical transduction, namely, electromechanical (EM) and optomechanical (OM) coupling. And $k_i(k_j)$ is the mechanical damping rate of the $i^{th}(j^{th})$ stage. C_{EM} is the cooperativity between the microwave and the mechanical resonator, and the C_{OM} is the cooperativity between the optical and the mechanical resonator.

1. *Calculating C_{EM}*

First, we calculate the C_{EM} using the expression

$$C_{EM} = \frac{4g_{EM}^2}{\gamma_m k_e}$$

where g_{EM} is the electromechanical coupling rate, γ_m is the mechanical energy loss rate (unit: Hz $\cdot 2\pi$), and k_e is the electrical decay rate (FWHM). The g_{EM} (unit: Hz $\cdot 2\pi$) can be extracted from the modeled effective circuit in [3]

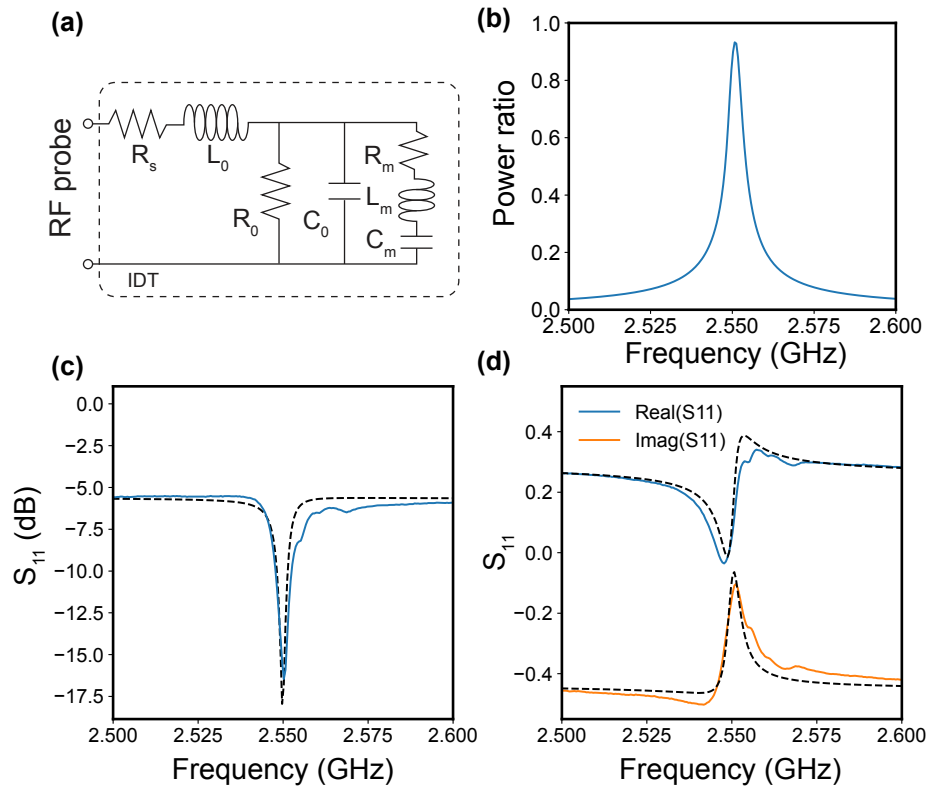

FIG. S4. **Fitting result of the modified BVD model at** 4 K **(a)** The BVD effective circuit that is used to model our piezoelectric system. **(b)** The power ratio that is loaded on the mechanical lumped elements. **(c)** The amplitude of the RF reflection spectrum of the measured IDT. The dotted line is the fitted result. **(d)** The real and imaginary part of the RF reflection spectrum of the measured IDT. The dotted line is the fitted result.

using

$$g_{EM} = \frac{\sqrt{k_T^2}\omega_m}{2}$$
$$k_T^2 = \frac{C_m}{C_m + C_0 + C_T}$$

where k_T^2 is the reduced piezoelectric coupling strength and $\omega_m = \omega_{LC}$ is the resonance frequency of the RF reflection spectrum. In our model, C_T is absorbed into C_0 since the two capacitors are connected in parallel. The modified Butterworth Van Dyke (BVD) model of the piezoelectric circuit for our system is shown in Fig. S4(a). The electrical decay rate k_e can be extracted from the FWHM of the RF reflection spectrum at resonance frequency, which is shown in Fig. S4(c).

We use the BVD model to fit the S_{11} data to extract C_0 and C_m. Fig. S4(c)(d) show the fitting result of the BVD model. The fitted $C_0 = 0.82\ pF$ and $C_m = 0.0013\ pF$. The fitting result is consistent with the measured data, and we use the extracted capacitance to calculate

$$k_T^2 = \frac{C_m}{C_m + C_0 + 0} = \frac{0.0013\ pF}{0.82\ pF + 0.0013\ pF} \sim 0.0016$$
$$\omega_m/2\pi = 2.556\ \text{(GHz)}$$
$$g_{EM} = \frac{\sqrt{k_T^2}\omega_m}{2} = 319.5\ \text{(Mrad/s)}$$
$$k_e = 15\ \text{MHz}$$
$$\gamma_m = 1.1\ \text{MHz}$$

and we can calculate the C_{EM} as:

$$C_{EM} = \frac{4g_{EM}^2}{\gamma_m k_e} = \frac{4 \cdot (319.5 \times 10^6)^2}{15 \times 10^6 \cdot 1.1 \times 10^6 (2\pi)^2} = 626$$

2. *Calculating C_{OM}*

Optomechanical cooperativity can be calculated as:

$$C_{OM} = \frac{4g_{OM}^2}{\gamma_m k_o}$$

where g_{OM} is the pump-enhanced coupling rate $g_{OM} = g_0\sqrt{n_{\text{phot}}}$, and n_{phot} is the intra-cavity photon number. The $g_0 = g$ is the single-photon optomechanical coupling rate, which can be calculated using the expression from section SI.1 from finite element analysis. Experimentally, g_0 can be extracted from the measured data and $\sqrt{n_{\text{phot}}}$ can be calculated from the optical pump power. γ_m can be extracted from the acoustic quality factor, and κ_0 can be extracted from the optical quality factor.

The phonon-flux normalized optomechanical coupling rate $g_{\text{extract}}/\sqrt{\hbar\Omega} = 230(\frac{1}{mm\sqrt{W}})$. We can write the pump-enhanced coupling rate as:

$$g_{OM} = g_0\sqrt{N_{phot}} = (\frac{g_{\text{extract}}}{\sqrt{\hbar\Omega}}\sqrt{P_a} \times \pi D) \times \sqrt{N_{phot}}$$

where D is the diameter of the OM ring, P_a is the RF pump power, and Ω is the acoustic mode frequency. We can calculate the optomechanical cooperativity using the above information:

$$\begin{aligned} g_0\sqrt{N_{phot}} &= (\frac{g_{\text{extract}}}{\sqrt{\hbar\Omega}} \times \sqrt{1.5 \cdot 10^{-3}} 200 \cdot 10^{-3}\pi)\sqrt{N_{phot}} \\ &= 5.7\sqrt{N_{phot}} \\ &= 293 \cdot 10^6 = g_{OM} \\ \gamma_m &= 1.1 \text{ MHz} \\ \kappa_o &= 20 \text{ pm} = 2.43 \text{ GHz at 1571 nm (loaded optical Q = 7.5e4)} \end{aligned}$$

and we can calculate the C_{OM} as:

$$C_{OM} = \frac{4g_{OM}^2}{\gamma_m k_e} = \frac{4 \cdot (293 \cdot 10^6)^2}{1.1 \cdot 10^6 \times 2.43 \cdot 10^9 (2\pi)^2} = 3.35$$

B. Transduction Efficiency

The conversion efficiency in the main text only considers the conversion of TE_0 to TE_2 modes, which is different from the transduction efficiency discussed here, namely the intrinsic efficiency η_i and the total efficiency η as shown in Fig. S3. The intrinsic transduction efficiency can be expressed as

$$\eta_{it} = \frac{\eta}{\eta_o \eta_e}$$

where $\eta_o = \eta_{02} \cdot \eta_{GC}$ is the optical coupling efficiency from the OM ring to the waveguide (η_{02}) and from the waveguide grating coupler to the optical fiber (η_{GC}). η_e is the electrical coupling efficiency and can be extracted from the lump elements [5].

$$\eta_e = \frac{Z_{tx}}{Z_{tx} + R_s}$$

where R_s is the series resistance of the IDT, as shown in Fig. S4. The $R_s = 19\ \Omega$, and $Z_{tx} = 50\ \Omega$, and the resulted $\eta_e = 0.72$. The total transduction efficiency η can be expressed as [4]:

$$\eta = \eta_o \eta_e \frac{4C_{OM}C_{EM}}{(1 + C_{OM} + C_{EM})^2} = 3.1\% \cdot 3\% \cdot 72\% \frac{4 \cdot 3.35 \cdot 626}{(1 + 3.35 + 626)^2} = 1.37 \cdot 10^{-5}$$

and the internal transduction efficiency $\eta_{it} = 2.1\%$.

C. Added noise

The added noise N arises from two main contributions in our platform: optical noise contributed by the stokes scattering N_o and the mechanical thermal noise from the pumped phonon N_m. The optical added noise can be expressed as:

$$N_o = \frac{1}{\eta_e}\frac{C_{OM}\mathcal{L}_-^2}{C_{EM}}$$

where the optical-cavity Lorentzian sideband amplitudes are expressed as

$$\mathcal{L}_\pm^2 = \frac{(\kappa_o/2)^2}{(\kappa_o/2)^2 + (\Delta \pm \omega_m)^2}$$

The Stokes sideband amplitude $\mathcal{L}_-^2 = 0.18$. We can use the information calculated so far to calculate optical added noise as:

$$N_o = \frac{1}{0.72}\frac{3.35 \cdot (0.18)}{626} = 0.0013$$

The mechanical thermal noise can be expressed as:

$$N_m = \frac{1}{\eta_e}\frac{n_m}{C_{EM}}$$

where $n_m(\omega) = [e^{\hbar\omega/(k_B T)} - 1]^{-1}$ is given by the Bose-Einstein distribution and $\omega = \omega_m$. We can calculate the mechanical thermal noise as:

$$N_m = \frac{1}{0.72}\frac{33}{626} = 0.07$$

And the total added noise is the sum of the two contributions:

$$N_{add} = N_o + N_m = 0.0713$$

SI.4. EXTRACTING ELECTROMECHANICAL CONVERSION EFFICIENCY AND CHARACTERIZING THE ACOUSTIC TRANSMISSION SIGNAL S_{21}

BVD model and electromechanical conversion efficiency of the IDT

The IDT's performance is modeled using the effective circuit shown in Fig. S4(a). The resistor R_s accounts for the total series resistance between the RF probe and the IDT fingers, and the inductor L_0 accounts for the inductive background signal in the cryogenic environment. The shunt resistor R_0 and the capacitor C_0 account for the effective leakage resistance and electrode capacitance between the IDT fingers, respectively. The electromechanical response of the transducer is modeled with a complex and frequency-dependent admittance $Y_m = R_m + 1/j\omega C_m + j\omega L$, as generalized from the BVD model [6]. To extract the IDT's electromechanical conversion efficiency, we use the BVD effective circuit, as shown in Fig. S4(a), to obtain the value of the circuit lump elements and calculate the power load on the motional elements. We can express the load impedance Z_{L} as:

$$Z_{\mathrm{L}} = R_s + j\omega L_0 + \left(\frac{1}{Z_0} + \sum_N Y_m^{(N)}(\omega)\right)^{-1} = \frac{1}{Y_{\mathrm{L}}}, \tag{SI.8}$$

where C_0 and R_0 are combined as effective load Z_0, and $L_m(\omega)$, $C_m(\omega)$, and $R_m(\omega)$ are combined as the mechanical elements at the target resonance frequency.

$$Z_0 = \frac{1}{j\omega C_0 + 1/R_0} \tag{SI.9}$$

$$Y_m(\omega) = \frac{1}{Z_m} = \frac{1}{R_m + j\omega L_m + 1/j\omega C_m}. \tag{SI.10}$$

Then, the power ratio corresponds to the power transfer to each lump components in the effective circuit. We perform the least square curve fit near the resonance peak ω and **exclude** the admittance (Y_m) element to obtain R_s, R_0, L_0 and C_0. The reason we can exclude the admittance (Y_m) is because that reflected power at resonance can be solely attributed to the effect of Y_m, which is a function of frequency ω. The total load impedance Z_L of the effective circuit after excluding Y_m then becomes

$$Z_L = R_s + j\omega L_0 + \frac{1}{Z_0},$$

and

$$Z_L = R_{char} \times \frac{1 + \mathbb{C}(S11(\omega))}{1 - \mathbb{C}(S11(\omega))}, R_{char} = 50\Omega$$

Note that S_{11} is a complex number, which can be extracted from the polar chart in the VNA. In this way, we can relate the measured S_{11} to the lumped elements. Experimentally, the IDTs are driven by an VNA that scans the RF frequency to extract the complex S_{11}, which we can use the above model to fit and derive the electromechanical conversion efficiency. The fitted electromechanical conversion efficiency is close to 90% at 4 K, as shown in Fig. S4(b).

Characterizing S_{21} signal

Generally, the time-gating signal processing is performed using the following steps: (1) inverse Fourier transform (IFT) of the frequency domain S_{21} to time domain, (2) gating the acoustic impulse respond and filter out the free-space interference in time domain, and (3) Fourier transform of the gated signal back to frequency domain. Fig. S5a shows the original RF transmission signal taken from the VNA. The inverse Fourier transform of the S_{21} signal is shown in Fig. S5b. We can see a much stronger signal at $t < 190$ ns; this is the free space radiation and the electronic background signal from the IDTs, so we filter out such a signal. Periodic sharp peaks that occur every 180 ns are also seen in the time-domain data, we attribute this to the reflection of bulk acoustic waves, which only contributes to an overall broadband background signal without distorting the main feature of the S_{21} resonance in frequency domain. We can also clearly see two impulse responses at 210 ns and 400 ns.

We focus on the two impulse responses at 200 ns and 400 ns. The first impulse corresponds to the L_2 mode that is directly traveling through the acoustic waveguide, whose path is shown in the inset of Fig. S5d, and the corresponding time-gated signal is shown in Fig. S5d. In this case, we can remove the free space RF crosstalk by filtering out the

signal < 190 ns. We can calculate the L_2 mode group velocity by dividing the waveguide length to the time of the first impulse signal, which yields $v_{L_2} = 760/220$ $\mu m/ns = 3454$ m/s, which is consistent with the simulation. The second impulse signal at 400 ns corresponds to the L_2 mode that is coupled into the ring and out, whose traveling path (1388 μm) is shown in the inset of Fig. S5c, which is consistent with the arrival time calculated v_{L_2}.

Finally, we gate the signal from $190 < t < 540$ ns, which corresponds to the superposition of the first and second pulse, as shown in Fig. S5c. The interference of the both pulses will result in the FSR that is similar to an optical ring resonator, where multiple passes of the optical wave from the ring interfere with each other resulting in the resonance dips in the transmission spectrum. Note that the Fourier and inverse Fourier transform are performed on a complex S_{21} data. The similar time-gating techniques are also described in other works [7][8].

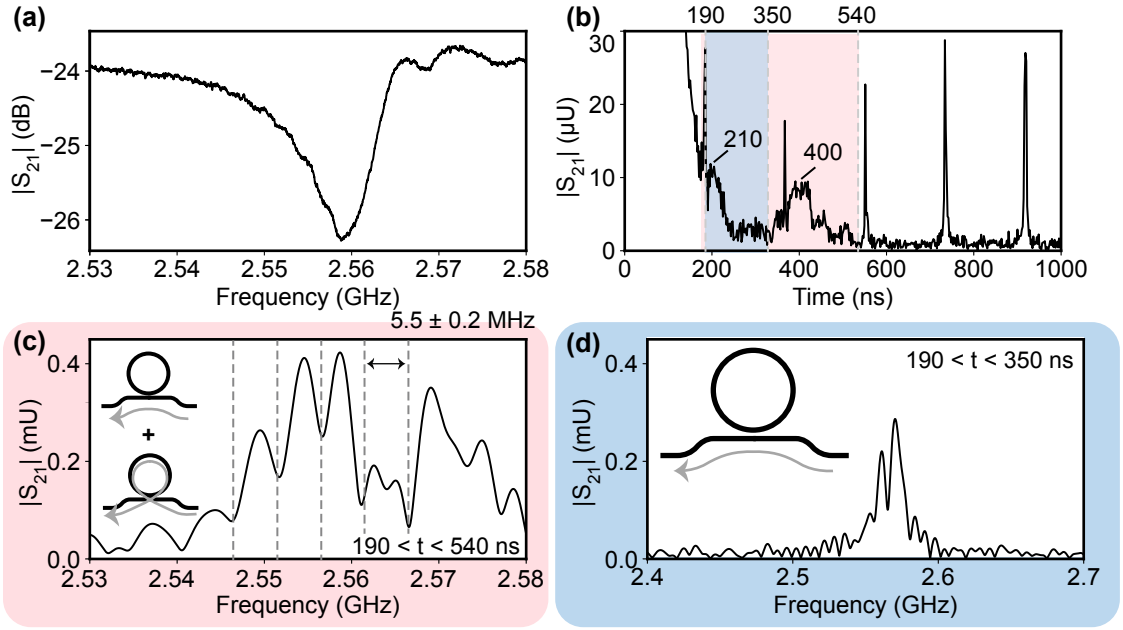

FIG. S5. **Time-gating signal processing of the acoustic transmission S_{21}. (a)** The unprocessed $|S_{21}|$ spectrum that is acquired from the VNA. **(b)** The $|S_{21}|$ in the time domain. **(c)** The $|S_{21}|$ spectrum that is time-gated from $190 < t < 540$ ns. The light (dark) gray dashed line shows equal spacing of 5.5 ± 0.2 MHz. The inset in **(c)** shows the acoustic traveling path within the gated time window. **(c)** is the data shown in the main text but zoomed in. **(d)** The $|S_{21}|$ spectrum that is gated from $190 < t < 350$ ns. The inset shows the acoustic wave traveling path within the gated time window.

SI.5. PHASE-MATCHING CONDITIONS OF ALL POSSIBLE PROPAGATION DIRECTIONS OF THE OMR

The PMC measurement setup for all possible OMR configurations is shown in Fig. S6a. Both the optical and acoustic pump are fixed at the OMR resonance. Totally, four acoustic ports for input and output are available. In addition, two optical input ports and two optical output ports are available to select the circulation direction of the optical modes. Therefore, we can investigate all possible configurations of acoustic and optical input/output at all possible ports to characterize the time-reversal symmetry of the OMR. When the RF power is turned off, we observe a linear static TE_2 mode whose source is described in the main text, as shown as the black line in Fig. S6. When the RF is turned on, we observe strong TE_2 mode intensities increase for all counter-propagating acoustic and optical waves. This is the result of the dominant anti-Stokes-Brillouin process in the OMR, which is shown in the red lines in Fig. S6b-f. For the co-propagation cases, which are shown in Fig. S6g-k, we observe an optical output intensity retaining or drop in the optical spectrum analyzer (OSA), which can be attributed to the reduction of the undesired generated TE_2 mode because the out-scattering of TE_0 mode by the dominating co-propagating acoustic waves.

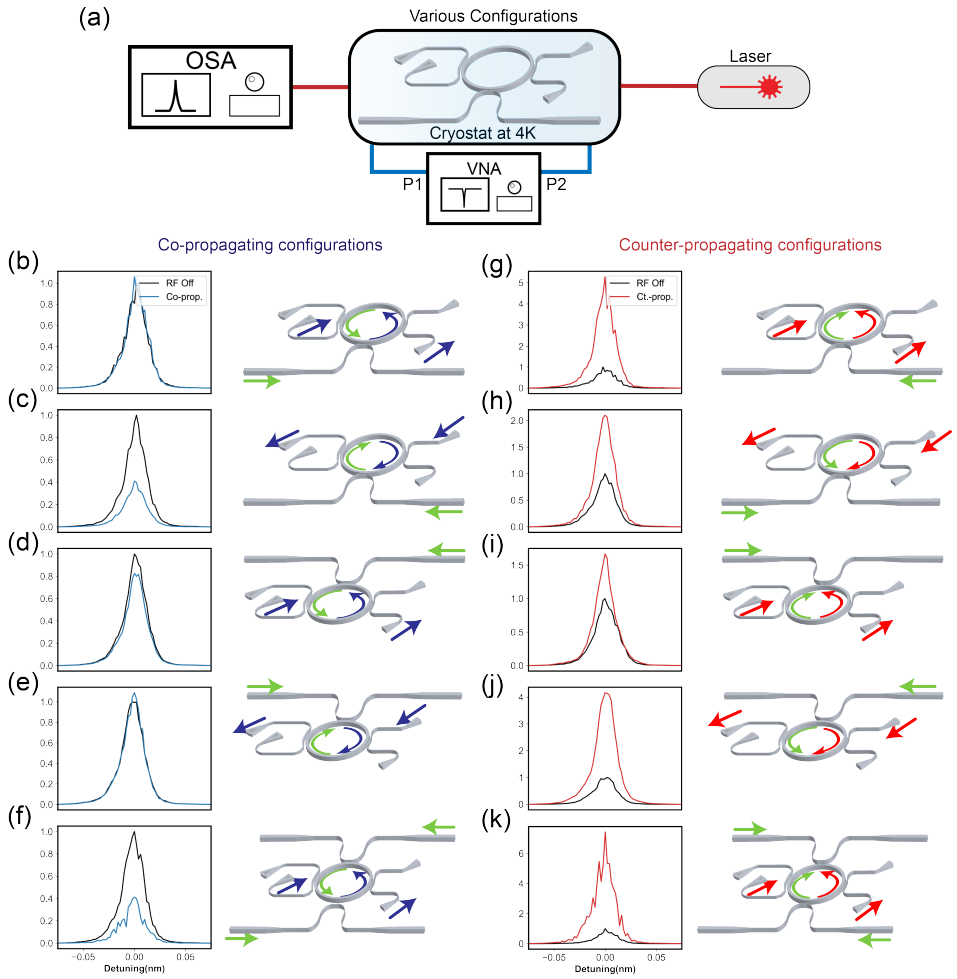

FIG. S6. **Phase-matching conditions of all co-propagating and counter-propagating configurations at cryogenic temperature. (a)** The measurement schematic of the PMC measurements. Both the laser and RF inputs are on resonance. Laser is fixed at resonance at 1571.67 nm and the RF driving at 2.56 GHz. The laser input is routed to the chip in the cryogenic probe station via the fiber probes and received at the OSA. **(b)-(f)** Shows the OSA spectrum with co-propagating configurations. **(g)-(k)** Shows OSA spectrum with counter-propagating configurations. Blue and red arrows show the co-propagating and counter-propagating optical waves, respectively. Green arrows show the acoustic wave propagation directions. The optical transmission for all the measurements shown here are normalized to the intensity when acoustic wave is turned off (black line).

SI.6. OMIC FABRICATION PROCESS FLOW

The OMIC fabrication process flow diagram is shown in Fig. S7.

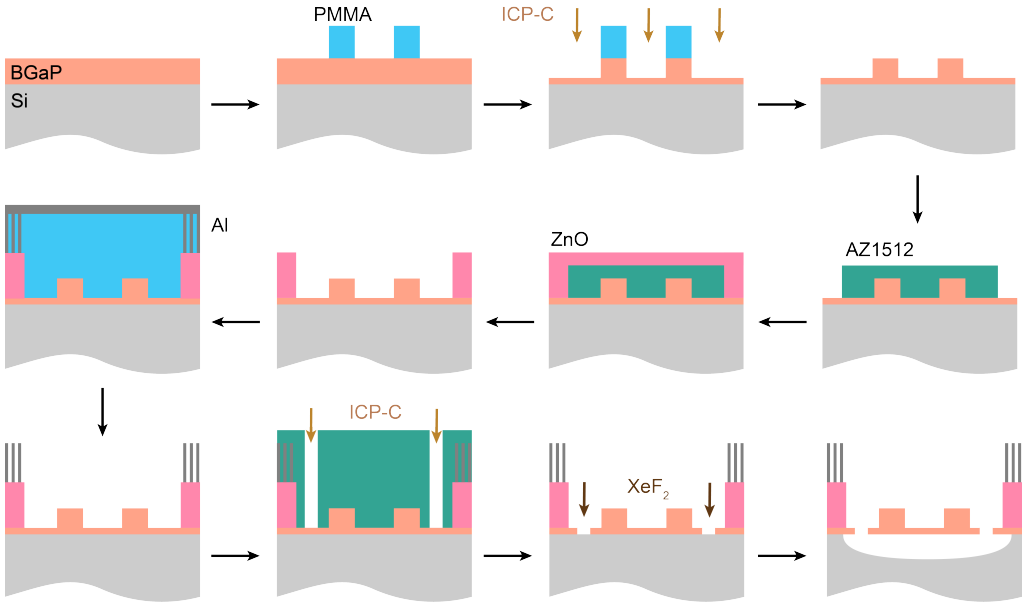

FIG. S7. **OMIC fabrication process flow.** We begin fabrication on a BGaP-on-Si chip and finished with a suspended BGaP film with ZnO and aluminum fingers on top. PMMA is patterned using EBL and AZ1512 photoresist is patterned using photolithography (Heidelberg DWL66+).

SI.7. DEVICE DESIGN PARAMETERS

More details of the device parameter are provided in the table. S3.

OMIC device parameters				
	Parameters	Unit	TE_0	TE_2
Multi-mode OMR	Wavenumber modes(β_i)	μm^{-1}	10.43	7.302
	Wavenumber difference ($\beta_0 - \beta_2$)	μm^{-1}	3.13	
	Effective mode index(n_{eff})		2.558	1.784
	Group index(n_g)		3.245	3.315
	Hybrid TE_0-TE_0* (Δn_{eff})		$2.567 - 2.554 = 0.013$	
	Multi and single mode waveguide width(w)	μm	1.01	0.50
	Ring diameter(D)	μm	200	
	Ring total length(l_{tot})	μm	628.318	
	Optical coupling length(L_{ii})	μm	$L_{00} = 50$	$L_{02} = 60$
	Optical coupling gap width(g_{ii})	μm	$g_{00} = 0.07$	$g_{02} = 0.20$
	Waveguide to OMR coupling efficiency(η_{ii})	%	$\eta_{00} = 90$	$\eta_{02} = 3$
	Single grating coupler efficiency(η_{GC})	%	3.1	
	Optical FSR	nm	1.142	1.08
	Parameters	Unit	L_2	
2nd-order Lamb mode (L_2)	Acoustic wave central frequency($\Omega/2\pi$)	GHz	2.56	
	Acoustic wavenumber(κ)	μm^{-1}	3.13	
	Acoustic waveguide width(w_a)	μm	1.01	
	Acoustic waveguide tapered length(l_a)	μm	100	
	Acoustic Coupling length(l_a)	μm	$l_a = \frac{2\pi}{\Delta K} = \frac{2\pi}{0.4} = 13$	
	Acoustic Coupling gap width(g_a)	μm	0.2	
	Simulated acoustic group velocity (V_g)	m/s	3424	
	Measured acoustic group velocity (V_g)	m/s	3450	
	Calculated Acoustic FSR	MHz	5.44	
	Measured Acoustic FSR	MHz	5.5	
	IDT pitch(Λ)	μm	2	
	IDT aperture(W)	μm	15	
	IDT efficiency(η_a)	%	$\sim$90	

TABLE S3. The phononic and photonic design parameters of the OMIC and OMR. *Δn_{eff} is the effective refractive index difference in the TE_0-to-TE_0 coupling region that the hybrid mode has phase differences π, which helps us calculate the coupling length needed for critical coupling.

[1] S. G. Johnson, M. Ibanescu, M. A. Skorobogatiy, O. Weisberg, J. D. Joannopoulos, and Y. Fink, "Perturbation theory for maxwell's equations with shifting material boundaries," *Phys. Rev. E*, vol. 65, p. 066611, Jun 2002.
[2] B. G. Mytsyk, N. M. Demyanyshyn, and O. M. Sakharuk, "Elasto-optic effect anisotropy in gallium phosphide crystals," *Applied Optics*, vol. 54, no. 8546-8553, 2015.
[3] M. Wu, E. Zeuthen, K. C. Balram, and K. Srinivasan, "Microwave-to-optical transduction using a mechanical supermode for coupling piezoelectric and optomechanical resonators," *Phys. Rev. Appl.*, vol. 13, p. 014027, Jan 2020.
[4] X. Han, W. Fu, C.-L. Zou, L. Jiang, and H. X. Tang, "Microwave-optical quantum frequency conversion," *Optica*, vol. 8, pp. 1050–1064, Aug 2021.
[5] M. Aspelmeyer, T. J. Kippenberg, and F. Marquardt, "Cavity optomechanics," *Reviews of Modern Physics*, vol. 86, pp. 1391–1452, dec 2014.
[6] H. Li, Q. Liu, and M. Li, "Electromechanical Brillouin scattering in integrated planar photonics," *APL Photonics 4, 080802*, 2019.
[7] M. Bicer, S. Valle, J. Brown, M. Kuball, and K. C. Balram, "Gallium nitride phononic integrated circuits platform for GHz frequency acoustic wave devices," *Appl. Phys. Lett.*, vol. 120, no. 243502, 2022.
[8] F. M. Mayor, W. Jiang, C. J. Sarabalis, T. P. McKenna, J. D. Witmer, and A. H. Safavi-Naeini, "Gigahertz Phononic Integrated Circuits on Thin-Film Lithium Niobate on Sapphire," *Phys. Rev. Applied*, vol. 15, Jan 2021.